A generalization of the Thickened Flame model for stretched flames

Nicola Detomaso[a], Jean-Jacques Hok[a], Omar Dounia[a], Davide Laera[b,a], Thierry Poinsot[c,a]

[a] *CERFACS, 42 avenue Gaspard Coriolis, 31057 Toulouse, France*
[b] *Departement of Mechanics, Mathematics and Management, Polytechnic University of Bari, Via Orabona, 70125 Italy*
[c] *IMFT, Allée du Professeur Camille Soula, 31400 Toulouse, France*

Abstract

The Thickened Flame (TF) model is a widely used approach for Large Eddy Simulation of premixed flames. It is based on a "mapping" transformation where all diffusivities are multiplied by a thickening factor F while reaction terms are divided by F. Theory shows and 1D flame simulations confirm that this mapping preserves the unstretched laminar flame speed s_L^0 while increasing its thickness δ_L^0 by F, allowing to resolve the flame on a coarse grid. However this property is not satisfied anymore when the TF model is applied to stretched flames: the burning velocity $s_c(k)$ of a thickened flame submitted to a stretch k is not conserved compared to the non-thickened solution. A new diffusion-reaction transformation, named Stretched-Thickened Flame (S-TF) model, is developed here to conserve the burning velocity of stretched flames, proposing a generalization of the classical diffusion-reaction transformation which the TF model is based on. Thermal and mass diffusion zones are thickened differently and the laminar unstretched properties

*Corresponding author: detomaso@cerfacs.fr

are preserved by modifying the chemical source terms. The S-TF model is applied on canonical 1D strained flames and validated for a cylindrical expanding flame configuration to prove its applicability to recover both strain and curvature effects. Results show that the Stretched-Thickened Flame model is an effective solution to correct the deficiency of the classical approach for stretched flames and can be easily implemented in CFD codes relying on the TF model.
Keywords: Stretched flames, Thickened Flame model, Consumption speed, Premixed laminar flames, CFD

Novelty and significance statement

- A Thickened Flame model generalization to correct stretched thickened flame behavior is proposed.
- When strained flames are thickened following the classical Thickened Flame model theory, its parameters such as the consumption speed are not retained.
- It is possible to demonstrate mathematically that a non-thickened flame reacts to the stretch k as the same thickened flame does to the stretch k/F.
- The proposed approach (Stretched-Thickened flame model) is developed starting from a generalization of the diffusion-reaction transformation of the Thickened Flame model.
- The model does not require the local evaluation of stretch on the flame front since it is based on a correction of the chemistry reactivity. In ad-

dition it guarantees the correct consumption speed of thickened flames from high to zero stretch.

- The model is validated both for strained and curved flames and its implementation in a CFD code is as simple as the classical Thickened Flame model.

Authors contributions

N.D.:designed research, performed research, analyzed data, wrote the paper. J.H.:performed research, analyzed data, reviewed the paper. O.D.:designed research, performed research, reviewed the data, reviewed the paper. D.L.: designed research, performed research, reviewed the data, reviewed the paper. T.P.:designed research, reviewed the data, reviewed the paper.

1. Introduction

Large Eddy Simulation (LES) is an effective and widely used approach when dealing with unsteady flames, at reasonable cost. Nevertheless, in reactive simulations, flames length-scales are smaller than the LES grids size, requiring specific combustion models [1]. The Thickened Flame (TF) model, inspired by the pioneering work of O'Rourke and Butler[2], addresses this issue by artificially increasing the flame thickness by a factor F, in order to solve the species and enthalpy/temperature transport equations on the computational grid, evaluating the chemical source terms with the finite rate kinetics approach [1]. Thanks to its simplicity, the TF model has gained attention from the combustion community, proving the capability to perform reliable simulations of turbulent premixed flames involving propagation [3–6], ignition [7, 8], stabilization mechanisms [9, 10], tabulated chemistry [11, 12], piston engines [13, 14], autoignition [15, 16], spray combustion [17].

For the 1D unstretched stationary flame, the TF formulation is exactly derived from a self-similar space-dilation transformation. However, its physical behavior, when departing from this canonical limit, is an open problem. For instance, several studies [11, 18–20] have shown that the application of a thickening factor can lead to an amplification of the stretch effect k on the flame. Indeed, as stated by Veynante and Poinsot [18] as soon as the model was derived, the thickened flame reacts to a stretch k/F as the fully resolved flame (i.e., $F = 1$) does to a stretch k: even though the actual flame is subjected to a small value of stretch, thickening amplifies the stretch effects on consumption speed [19] or quenching [21]. Although this statement can be verified in laminar flames, the stretch effect on thickened flame fronts

subjected to a turbulent field is not of minor importance. As highlighted by Comer et al. [21], the efficiency functions [1, 22, 23] used to recover the flame wrinkling reduced by the thickening process, are built to model subgrid scales and do not take into account resolved-stretch effects such as the curvature of an expanding ignited kernel or the high velocity gradient experienced by flames in a jet in a cross flow configuration. This is a major issue: in LES, the propagation speed of the resolved premixed front should be equal to $Es_c(Y_i, T)$ [24] where E is the efficiency function and s_c the laminar flame consumption speed (or burning velocity), depending on the mass fraction of the $i-$species (Y_i) and temperature (T). Unfortunately, this property is not true if the resolved front is stretched, something which occurs in most flames. This systematic error of the TF model approach is not acceptable as it wastes most of the interests of the method: even if chemical schemes have been built to match the unstretched flame properties within a few percent, the combination of thickening and stretch will induce errors of the order of 50% [19, 21] on the laminar flame burning velocity $s_c(Y_i, T)$. Similarly, even though the efficiency functions used to describe flame/turbulence interaction were perfect, the resolved, thickened flame, when stretched, would not propagate at the right speed ($Es_c(Y_i, T)$). This explains recent interest in stretched, thickened flames [4, 19, 21, 25] as well as the goal of this paper.

Recent works have proposed different solutions to retrieve the correct stretch response of thickened flames. Han et al. [11] coupled the TF model with a tabulated chemistry based on strained premixed flamelets to simulate a turbulent premixed jet flame at high Karlovitz number. Proch and Kempf [20] extended the premixed flamelet generated manifolds technique

with a correction based on local strain rates, showing a positive impact on the flame length. Popp et al. [19] introduced a strained-based function inside the diffusion term of the governing equations of premixed flames in stagnation point flow to correct the effect of the convection budget, once the TF model transformation is applied.

All the mentioned approaches, trying to correct the limitations of the classical TF model, have been developed in the context of tabulated chemistry and, while in [11] the strain effects are taken into account by tabulating H-radicals mass fractions [26], all the others require the computation of the local instantaneous stretch rate, which is not straightforward: this task requires dedicated mathematical operators to compute the velocity tensor as well as the flame normal. Furthermore, even if this is correctly accomplished during the simulation, the thickened flame may require an adaptation time when submitted to a certain instantaneous stretch field, which may demand additional correction factors [19]. Alternatively, Comer et al. [21], proposed a modification of the mixture Lewis number obtained through an optimization method based on Twin Premixed CounterFlow flames (reactants-to-reactants configuration) to match the extinction strain rate of the thickened flames. This procedure avoids real time computation of stretch during LES but the flames consumption speed, at different strain values, is not guaranteed. A similar approach was proposed in the TF-adapt model developed by Quillatre [4] and recently improved in the work of Poncet et al. [25] to ensure the Markstein length conservation at low stretch when thickening is applied. The TF-adapt model, however, fails to correctly reproduce the flame characteristics at high stretch values where asymptotic theory is not valid anymore.

To our knowledge, no previous works have shown an alternative formulation of the TF model to retrieve the correct response of thickened flames over a wide range of stretch, independently of the stretch level and avoiding the local evaluation of the strain rate and/or curvature in the LES. In this work, a novel approach named Stretched-Thickened Flame model (S-TF) is proposed to address these needs, so that, stretch effects on thickened premixed flame elements can be correctly captured when resolved on LES grid.

Section 2 provides an overview of the classical Thickened Flame model to introduce the background required for the definition of strain effects on thickened flames. Section 3 presents the new S-TF model to correctly predict the thickened flames behavior when subjected to strain. Section 4 reports the validation tests for strained and curved flames.

2. Problem formulation and motivations

2.1. Thickened Flame model for unstrained laminar flames

The Thickened Flame model is an attractive solution to propagate a premixed flame on a coarse grid. Butler and O'Rourke [2, 27] laid the theoretical foundation of the model, proposing the introduction of a coordinate dilatation ($x \mapsto x^*$) normal to the flame front:

$$x^* = \int^x F dx', \tag{1}$$

where F is the thickening factor.

For a single-step reaction[1] where the reactant R is converted into product P [24], the following governing equations for fuel mass fraction Y_F and

[1]The simple step assumption is used here to simplify the notation.

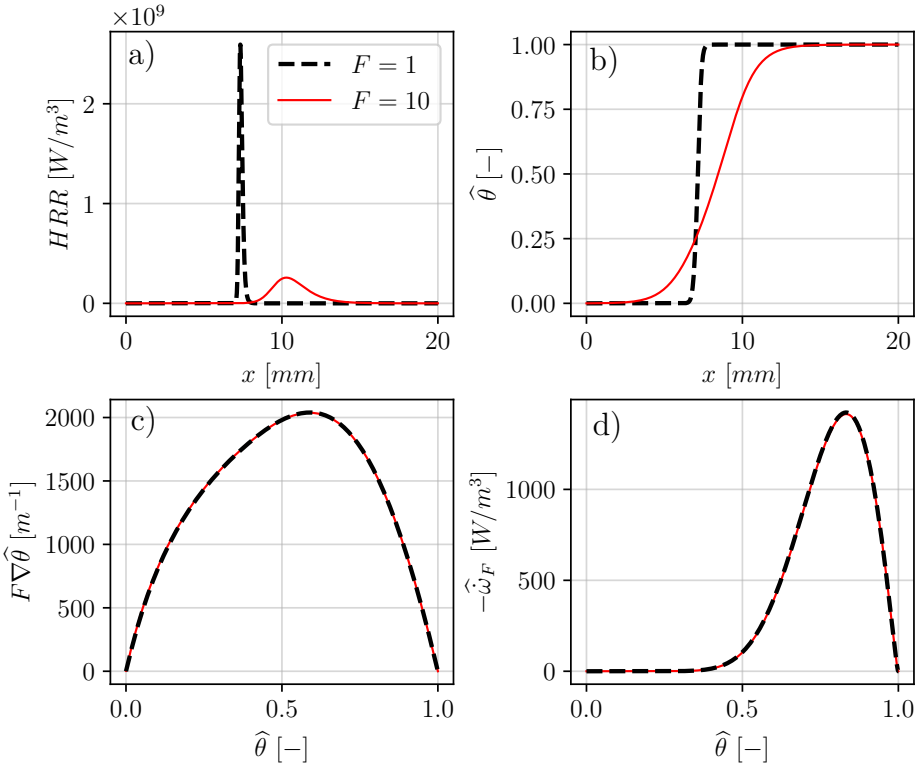

Figure 1: Classical TF model applied to unstrained flames with $F = 1$ and $F = 10$. a) Heat release rate in coordinate x. b) Progress variable $\widehat{\theta}$, mapped with Eq. (7), in space coordinate x. c) Progress variable gradient in the temperature domain. d) Fuel source term in the temperature domain.

temperature T are obtained:

$$\frac{\partial}{\partial t}\left(\rho Y_F\right) + \frac{\partial}{\partial x_j^*}\left(\rho u_j Y_F\right) = \frac{\partial}{\partial x_j^*}\left(\rho F D_F \frac{\partial Y_F}{\partial x_j^*}\right) - \frac{\dot{\omega}}{F} \tag{2}$$

$$\frac{\partial}{\partial t}\left(\rho T\right) + \frac{\partial}{\partial x_j^*}\left(\rho u_j T\right) = \frac{\partial}{\partial x_j^*}\left(\rho F D_{th} \frac{\partial T}{\partial x_j^*}\right) + \frac{Q}{c_p}\frac{\dot{\omega}}{F} \tag{3}$$

where ρ is the density, u_j the $j-$component of velocity, D_{th} the thermal diffusivity, D_F the fuel mass diffusivity, $\dot{\omega}$ is the reaction rate and Q is the heat of reaction. As highlighted in [2], the equations are self-similar with

respect to the coordinate transformation: the resulting thickened flame solution is equivalent to the original one. Introducing with $\widehat{\bullet}$ the flame variables obtained with the model transformation, the laminar flame speed of the thickened flame is conserved ($\widehat{s_L^0} = s_L^0$), since the integral of the heat release rate is retained (Fig. 1a) and the laminar flame thickness, computed through the flame temperature profile [24] between the unburnt mixture at T^u and the burnt products at T^b,

$$\delta_L^0 = \frac{T^b - T^u}{max|\nabla T|}, \tag{4}$$

is increased by a factor F: $\widehat{\delta_L^0} = F\delta_L^0$. This is shown in Fig. 1b, where the normalized temperature θ:

$$\theta = \frac{T - T^u}{T^b - T^u} \tag{5}$$

is evaluated in space with $F = 1$ and $F = 10$. These results match scaling laws coming from asymptotic premixed flame theory [24]:

$$\begin{cases} s_L^0 \propto \sqrt{D_{th}\dot{\omega}} \Rightarrow \widehat{s_L^0} = s_L^0 \propto \sqrt{FD_{th}\dot{\omega}/F}, \\ \delta_L^0 \propto \frac{D_{th}}{s_L^0} \Rightarrow \widehat{\delta_L^0} = F\delta_L^0 \propto \frac{FD_{th}}{s_L^0}. \end{cases} \tag{6}$$

Thus, in the canonical TF model, the diffusion coefficients are increased by F while the source terms are reduced by the same factor F. This transformation is denominated here "mapping":

$$(D_k, D_{th}, \dot{\omega}_k) \mapsto (D_k F, D_{th} F, \dot{\omega}_k / F), \tag{7}$$

where D_k is the diffusion coefficient and $\dot{\omega}_k$ the source term of the species k. A convenient method to explain the s_L^0 conservation is to plot the flame structure in the reduced temperature space θ. The mapping of Eq. (7) ensures

that gradients are perfectly scaled by the thickening factor such that $F\nabla\widehat{\theta} = \nabla\theta$ (Fig. 1). This guarantees that the consumption speed [19, 24]:

$$\widehat{s_c} \propto \int \dot{\omega}_F dx = \int \frac{\dot{\omega}_F(\theta)}{F\nabla\widehat{\theta}} d\theta \tag{8}$$

corresponds exactly to s_L^0 for laminar unstrained flames, since $\dot{\omega}_F(\theta)$ is unchanged (Fig. 1d) and $F\nabla\widehat{\theta} = \nabla\theta$: the flame is thickened and burns locally less, conserving the integral of the heat release rate. This property is not rigorous for strained flames as discussed in the next section.

2.2. Strained laminar flames and numerical configuration

The combined effect between stretch and thickening are analyzed now using 1D strained flames results. This section details the computations setup.

When a premixed flame experiences a stretch k (strain k_s and/or curvature k_c), its consumption speed usually departs from the laminar flame speed s_L^0. For small values of k, asymptotic analysis [28, 29] gives the following linear relation:

$$s_c = s_L^0 - \mathcal{L}_c k \tag{9}$$

where $\mathcal{L}_c$ is the consumption Markstein length [30–37]. Nevertheless, applying the classical TF model to strained flames leads to a different behavior compared to Eq. (9).

Popp et al. [19] considered a stagnation point flame where reactants and products are injected respectively from the two extreme sides of the domain (Fig. 2). This configuration, also known as CounterFlow Premixed Flame (CFPF), is used here to understand the problem from a theoretical point of view and to simulate how strain and thickening affect premixed flames[2].

[2]Hawkes et al. [38] highlighted the physical reliability of this configuration for a flamelet

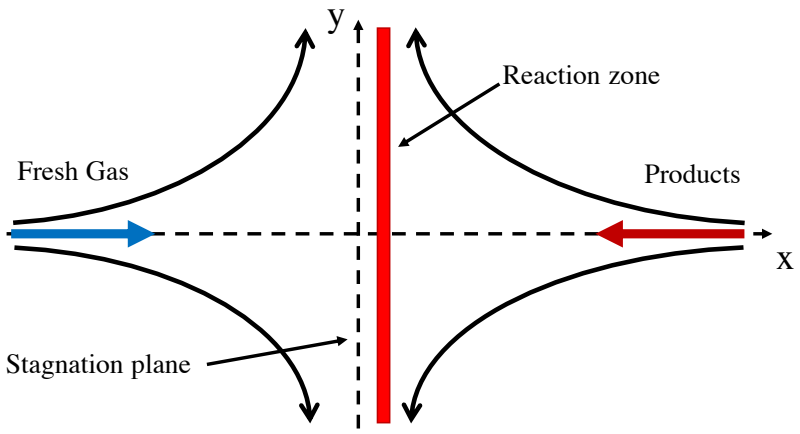

Figure 2: The CounterFlow Premixed Flame (CFPF): flame in a stagnation point flow. Reactants and products are injected respectively from the two extreme sides of the domain.

Stretch effects will be evaluated through the flame consumption speed, defined by [24]:

$$s_c = -\frac{1}{\left(Y_F^u - Y_F^b\right)\rho^u} \int \dot{\omega}_F dx \tag{10}$$

where Y_F^u and Y_F^b are the fuel mass fraction respectively in the unburnt and burnt gases while ρ^u is the density of the fresh mixture. A global approximation of strain rate (k_s), based on the injection velocity of fresh (U^u) and burnt gases (U^b), is used:

$$k_s = \frac{\mid U^u \mid + \mid U^b \mid}{L} \tag{11}$$

with L the length of the computational domain and the distance between the two injection points.

approach, showing that the CFPF is a coherent representation of the laminar flame structure embedded within a turbulent strained flame.

	$\phi_{0,j}$	$\sigma_{0,j}$	b_j	$\phi_{1,j}$	$\sigma_{1,j}$	c_j	$\phi_{2,j}$	$\sigma_{2,j}$	$\phi_{3,j}$	$\sigma_{3,j}$
$j=1$	1.180	0.039	0.25	1.2	0.02	27.8	1.64	0.14	–	–
$j=2$	1.146	0.046	0.00015	1.2	0.04	0.025	1.215	0.03	1.32	0.09

Table 1: PEA coefficients of the correction functions in Eqs. (14) and (15).

Strained flames simulations are carried out with CANTERA (https://cantera.org/) using a two-step chemistry for propane-air (C_3H_8/Air) combustion [39] :

$$C_3H_8 + 3.5O_2 \rightarrow 3CO + 4H_2O \tag{12}$$

$$CO + 0.5O_2 \rightleftharpoons CO_2 \tag{13}$$

where the first reaction determines the laminar flame speed while the $CO - CO_2$ equilibrium controls the adiabatic flame temperature. Inspired by the work of Franzelli et al. [40, 41], the Pre-Exponential Adjustment (PEA) technique is used to adjust the forward reaction rates for the two reactions ($k_{f,1}$,$k_{f,2}$) and reproduce the laminar flame speed in rich conditions:

$$k_{f,1} = K_{r,1} f_1(\phi) e^{(-E_{a,1}/RT)} \left[C_3H_8\right]^{n_{C_3H_8}} \left[O_2\right]^{n_{O_2,1}} \tag{14}$$

$$k_{f,2} = K_{r,2} f_2(\phi) e^{(-E_{a,2}/RT)} \left[CO\right]^{n_{CO}} \left[O_2\right]^{n_{O_2,2}} . \tag{15}$$

The following correction functions are used:

$$f_1 = \frac{2}{\left[1 + \tanh\left(\frac{\phi_{0,1}-\phi}{\sigma_{0,1}}\right)\right] + b_1\left[1 + \tanh\left(\frac{\phi-\phi_{1,1}}{\sigma_{1,1}}\right)\right] + c_1\left[1 + \tanh\left(\frac{\phi-\phi_{2,1}}{\sigma_{2,1}}\right)\right]} \tag{16}$$

$$f_2 = \frac{1}{2}\left[1 + \tanh\left(\frac{\phi_{0,2}-\phi}{\sigma_{0,2}}\right)\right] + \frac{b_2}{2}\left[1 + \tanh\left(\frac{\phi-\phi_{1,2}}{\sigma_{1,2}}\right)\right] + \\ + \frac{c_2}{2}\left[1 + \tanh\left(\frac{\phi-\phi_{2,2}}{\sigma_{2,2}}\right)\right]\left[1 + \tanh\left(\frac{\phi_{3,2}-\phi}{\sigma_{3,2}}\right)\right] . \tag{17}$$

	K_r $[cm^3/mol \cdot s]$	E_a $[cal/mol]$
C_3H_8 *oxidation*	2.534×10^{11}	3.27×10^4
$n_{C_3H_8} = 0.845,$		
$n_{O_2,1} = 0.631$		
$CO - CO_2$ *equilibrium*	2.0×10^9	1.2×10^4
$n_{CO} = 1.0,$		
$n_{O_2,2} = 0.5$		

Table 2: Summary of Arrhenius kinetic constants: K_r is the pre-exponential factor and E_a is the activation energy. n_k is the reaction exponent relative to the species k.

The two functions (f_1 and f_2) coefficients are summarized in Table 1 while the pre-exponential factor K_r and the activation energy E_a are reported in Table 2.

The fresh mixture conditions are taken at 1 *bar* and 300 K with an equivalence ratio $\phi = 0.9$. The transport used is based on a constant non-unity Lewis number [3, 4, 40]: with a Lewis number larger than one ($Le_k = 1.4$ with same Schmidt number among all the species and constant mixture Prandtl number [40, 41]), the flame characteristics are close to those obtained using the GRI-Mech3.0 detailed mechanism [42], for these operative conditions (Fig. 3a, $F = 1$ curve), providing a reliable prediction also for strained cases. Flame response will be examined for different values of k_s, by increasing the injection velocity. The domain length L is close to $100\delta_L^0$ to avoid flame-boundaries interactions.

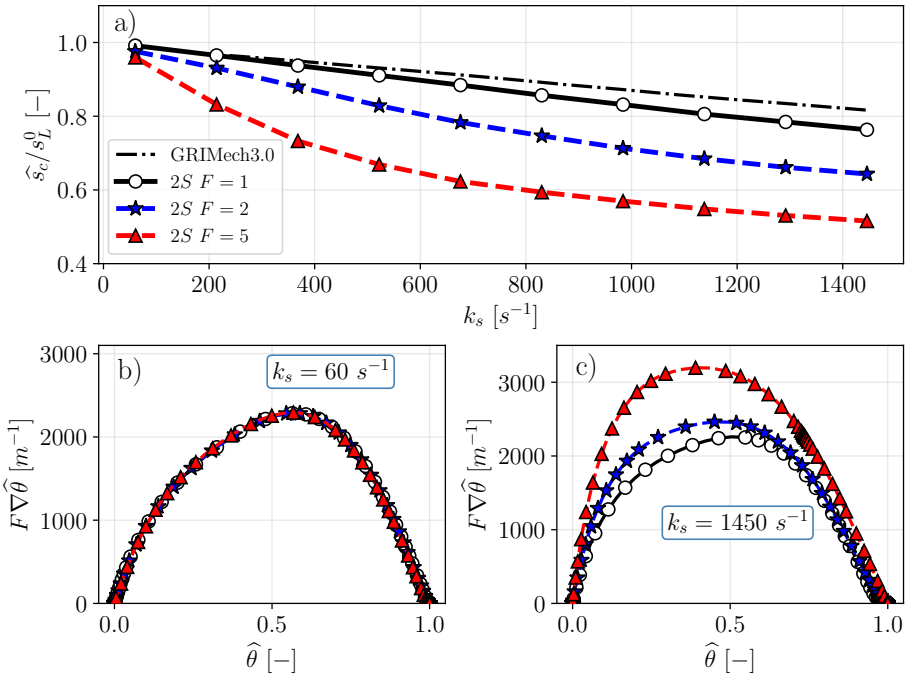

Figure 3: TF model applied to strained flames with $F = 1$, $F = 2$, $F = 5$. The flame at $F = 1$ obtained with the 2-step mechanism (here defined 2S) is compared with the GRI-Mech3.0. a) Normalized consumption speed behavior with respect the applied strain rate. b) Gradient of the progress variable at $k_s = 60\ s^{-1}$ vs temperature $\widehat{\theta}$. c) Gradient of the progress variable at $k_s = 1450\ s^{-1}$ vs temperature $\widehat{\theta}$.

2.3. Thickened Flame model application to strained flames

Previous works [19] proved that a thickened CFPF under the diffusion-reaction transformation (Eq. (7)) does not conserve its burning velocity $\widehat{s_c}$. This is verified here in Fig. 3a, where the consumption speed of the strained flames deviates from the exact value ($F = 1$) as soon as $F > 1$. The error increases both with thickening factor F and strain k_s. This is confirmed by the F-scaled gradient profiles of $\widehat{\theta}$ shown in Fig. 3(b-c). For very small strain values ($k_s = 60\ s^{-1}$) and relatively low values of F, (Fig. 3b), the

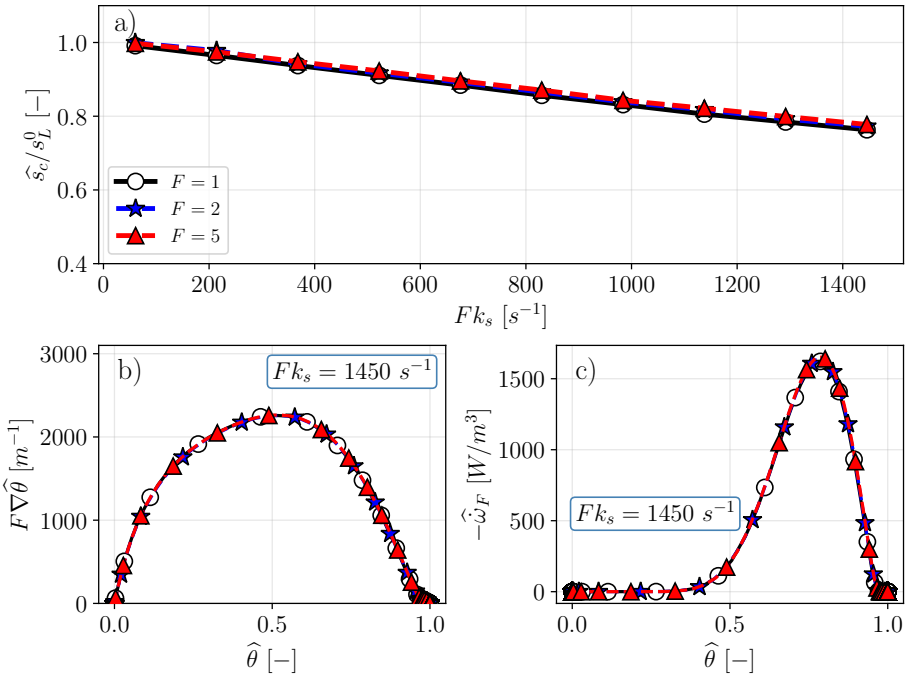

Figure 4: TF model applied to strained flames by applying the convection-diffusion-reaction transformation $(k_s, D_k, D_{th}, \dot{\omega}_k) \mapsto (k_s/F, D_k F, D_{th} F, \dot{\omega}_k/F)$. a) Consumption speed of the transformed flames normalized with s_L^0 and compared with the solution at $F = 1$. b) Gradient of the progress variable at $Fk_s = 1450\ s^{-1}$ versus the flames normalized temperature. c) Fuel source terms versus the normalized temperature at $Fk_s = 1450\ s^{-1}$.

flame structures exhibit a weak sensitivity to thickening and the consumption speed remains close to the reference value at $F = 1$ as for the classical TF model in the unstrained laminar case. The picture is different when strain is increased (Fig. 3c): $F\nabla\widehat{\theta}$ is not conserved in the temperature domain $\widehat{\theta}$ and, accordingly, the consumption speed diverges (see Eq. (8)) from the reference solution at $F = 1$. The mismatch becomes higher by increasing the thickening value.

This behavior has been explained in [19] and is briefly recalled here for completeness. By applying the coordinate change of Eq. (1) to the governing equations of a flame in a stagnation point flow, written on the centerline (e.g., x-axis) of the physical domain (Fig. 2), yields:

$$-\rho^u \frac{k_s}{F} x^* \frac{dY_F}{dx^*} = \frac{d}{dx^*}\left(\rho F D_F \frac{dY_F}{dx^*}\right) - \frac{\dot{\omega}}{F} \tag{18}$$

$$-\rho^u \frac{k_s}{F} x^* \frac{dT}{dx^*} = \frac{d}{dx^*}\left(\rho F D_{th} \frac{dT}{dx^*}\right) + \frac{Q}{c_p}\frac{\dot{\omega}}{F}. \tag{19}$$

Contrary to the unstrained case (Eqs. (2) and (3)), the factor F now appears also in the convection term of the equations due to the spatial variation of axial mass flux across the flame front, generating a strained flame.

Equations (18) and (19) suggest a more complex mapping than Eq. (7), preserving the flame structures and, thus, all flame properties:

$$(k_s, D_k, D_{th}, \dot{\omega}_k) \mapsto (k_s/F, D_k F, D_{th} F, \dot{\omega}_k/F). \tag{20}$$

Figure 4a displays the flames burning velocities computed for the three flames at $F = 1$, $F = 2$ and $F = 5$ by keeping Fk_s constant for all of them. The laminar flame speed conservation found for the unstrained flame (Fig. 1) is obtained, in this case, for the consumption speed of the strained solutions through the mapping of Eq. (20) as illustrated in Fig. 4b and Fig. 4c. Thus, as expected, a strained thickened flame reacts to a strain k_s/F exactly as a non-thickened flame does to a strain k_s (Fig. 4): in other words, the diffusion-reaction transformation of Eq. (7) generates flames reacting to a strain equal to Fk_s.

Although the transformation of Eq. (20) is an exact solution for the CFPF problem described in Fig. 2, it is by no means a general solution for simulation

of strained flames since the transformation $k_s \mapsto k_s/F$ derives directly from the potential flow assumption adopted to get Eqs. (18) and (19) and cannot be implemented in practice in other flow topologies where k_s is imposed by the flow. The mapping of Eq. (20) is therefore not a practical solution to correct stretch effects in CFD codes. A review of alternative solutions is proposed in the next section together with the development of the Stretched-Thickened Flame model.

3. Thickened Flame model extensions for strained laminar flame

A brief overview of previously proposed models is summarized in Table 3. Popp et al. [19] suggested a correction function based on strain rate, plugged inside the diffusion term of the temperature conservation equation (Eq. (19)) in order to recover flame gradients and, therefore, flame speed. Although it provides the exact burning velocity through a local flame structure adjustment, this approach demands the strain rate computation. The k evaluation is not immediate in a LES simulation of turbulent flames since it requires specific velocity field treatments, further assumptions and modelling.

A different approach relies on asymptotic theory [28]. In a first-order approximation, the consumption speed of weakly stretched flames is a function of the Lewis number of the mixture, the stretch k, and the resolved laminar flame thickness $F\delta_L^0$:

$$1 - \frac{\widehat{s_c}}{s_L^0} \propto F\delta_L^0 \left(Le^0 - 1\right) k \tag{21}$$

Equation (21) confirms that thickening the flame by factor F increases the slope of the function $\widehat{s_c}/s_L^0 = f(k)$ (Fig. 3a). However, the same relation

Model	Mapping	Speed matched	Properties conserved
TF [2]	$(D_k, D_{th}, \dot{\omega}_k) \mapsto (D_k F, D_{th} F, \dot{\omega}_k / F)$	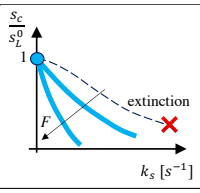	$s_c(k_s = 0)$
Popp [19]	$(D_k, D_{th}, \dot{\omega}_k) \mapsto (D_k F, \alpha D_{th} F, \dot{\omega}_k / F)$	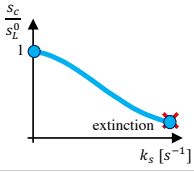	$s_c \; \forall \; k_s$ but k_s must be known
TF-adapt [4]	$(D_k, D_{th}, \dot{\omega}_k) \mapsto (D_k F_{sp}, D_{th} F_{th}, \dot{\omega}_k / F_r)$	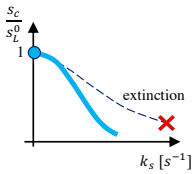	$s_c(k_s = 0)$, $\frac{\partial s_c}{\partial k_s}$ at $k_s \mapsto 0$ for a linear behavior
Comer [21]	$(D_k, D_{th}, \dot{\omega}_k) \mapsto (D_k F^{2-x_0}, D_{th} F^{2-x_0}, \dot{\omega}_k / F^{x_0})$	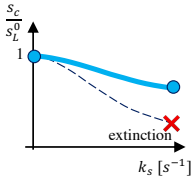	$s_c(k_s = 0)$, $k_s = k_s^{extinc.}$, $s_c(k_s^{extinc.})$ not guaranteed
S-TF	$(D_k, D_{th}, \dot{\omega}_k) \mapsto (D_k F_{sp}, D_{th} F_{th}, \dot{\omega}_k / F_r)$	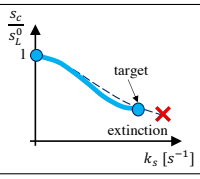	$s_c(k_s = 0)$, $s_c(k_s = k_s^{target})$, $\frac{\partial s_c}{\partial k_s}(0 \geq k_s \geq k_s^{target})$

Table 3: Methods comparison.

may be seen from another point of view: it reveals that for a given value of stretch k, the flame acts as if its Lewis number, or rather, $(Le^0 - 1)$ is modified. This observation was the basis of the TF-adapt solution developed by Quillatre [4] who proposed to artificially modify the species Lewis number in order to correct the stretch flame response. However, since it is based on

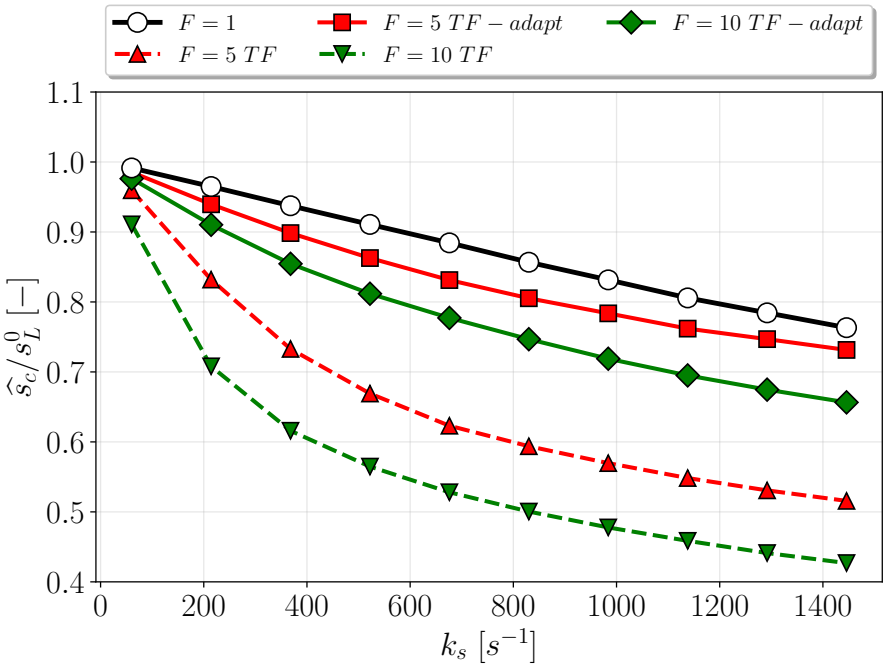

Figure 5: C_3H_8/Air flame consumption speed computed with the TF model and the TF-adapt approach in the CFPF configuration. Operative conditions: $P = 1\ bar$, $T = 300\ K$ and $\phi = 0.9$.

asymptotic theory [28, 29] the success of this approach depends on restrictive hypotheses such as low stretch, single-step chemistry and high Zel'dovich number. Recently, Poncet et al. [25] improved this theory with a Markstein length adjustment but still valid for only small stretch values.

Finally, Comer et al. [21] also suggested a Lewis number modification aiming mainly at matching the extinction strain rate k_s^{extinc}. However, this correction does not guarantee the consumption speed of the flame at all strain values. In a flamelet approach, the stretched flame regions would not burn as expected.

Figure 5 shows the flame consumption speed obtained with the TF and with the TF-adapt models in a 1D CFPF. As expected, the classical Thickened Flame model fails even for small thickening factors especially at high strains since the flame reacts to Fk_s. TF-adapt improves the flame stretch response but it guarantees the expected flame behavior only if the thickening factor is kept low. For high strain, the linear theory does not hold anymore and an error larger than 10% is observed.

From this review, it is possible to conclude that another approach is required in order to improve the flame transformation when the TF and the TF-adapt models show limitations. The Lewis number modification appears to be a convenient solution to correct the behavior of a stretched thickened flame, especially because it is based on chemistry response and does not require strain or curvature evaluation on the flame front.

A Lewis number optimization is proposed now, starting from a generalization of the diffusion-reaction transformation (Eq. (7)), in order to retrieve the correct flame stretch response regardless of the stretch values. The next section presents the mathematical formulation of this theoretical approach, leading to the definition of the Stretched-Thickened Flame model.

3.1. Generalization of the diffusion-reaction transformation: introduction of the Stretched-Thickened Flame (S-TF) model

The first step of the model is to recognize that differently from the classical Thickened Flame model, thermal diffusion D_{th} and species mass diffusion D_k can be scaled using different factors F_{th} and F_{sp} such that $\widehat{D_{th}} = F_{th}D_{th}$

and $\widehat{D_k} = F_{sp} D_k$. As a consequence, the Lewis number is changed as follow:

$$\widehat{Le} = \frac{\widehat{D_{th}}}{\widehat{D_k}} = \frac{F_{th} D_{th}}{F_{sp} D_k} = \frac{F_{th}}{F_{sp}} Le^0. \tag{22}$$

Since this Lewis number modification alters the unstretched laminar flame speed, a correction function F_r is applied to the Arrhenius pre-exponential factors to conserve s_L^0. This procedure leads to a generalization of the mapping introduced by the classical TF transformation of Eq. (7):

$$(D_k, D_{th}, \dot{\omega}_k) \mapsto (F_{sp} D_k, F_{th} D_{th}, F_r \dot{\omega}_k) \tag{23}$$

which, as announced, does not take into account the local value of strain.

The factors F_{th}, F_{sp}, F_r are unknown a priori: their values can be determined by targeting three specific flame properties. First, the unstretched flame quantities must satisfy:

$$\frac{\widehat{s_L^0}}{s_L^0} = 1 \tag{24}$$

$$\frac{\widehat{\delta_L^0}}{\delta_L^0} = F \tag{25}$$

where $\widehat{s_L^0}$ and $\widehat{\delta_L^0}$ represent the unstretched laminar flame speed and thickness once the generalized transformation of Eq. (23) is applied. Equation (24) and (25) guarantee the unstretched laminar flame speed conservation and the thermal thickness resolution, respectively, as obtained through the classical Thickened Flame model.

Equations (25) imposes the thermal diffusion factor F_{th}:

$$\frac{\widehat{\delta_L^0}}{\delta_L^0} = \frac{\widehat{D_{th}}}{\widehat{s_L^0}} \frac{s_L^0}{D_{th}} = F_{th} = F, \tag{26}$$

showing that, in the S-TF model, the thermal diffusion is still increased by F.

The first constraint (Eq. (24)) is now used to find F_r. Following premixed flame theory [24, 43], the laminar flame speed depends on the square root of the reaction pre-exponential factor (K_r) and on thermal diffusion and species mass diffusivity:

$$s_L^0 \propto K_r^{1/2} D_{th}^{\alpha} D_k^{\beta}, \tag{27}$$

where α and β are parameters that generalize the laminar flame speed dependency on D_{th} and D_k, or, in other words, on the Lewis number. They are obtained from unstretched laminar flame properties and classical theory for non-unity Lewis number shows that their sum is equal to 1/2: $\alpha + \beta = 1/2$. The procedure to compute them is detailed in Appendix A. Differently from other formulations [24], no hypothesis on the complexity of the chemical scheme has been used in Eq. (27). The laminar flame speed ratio may therefore be expressed as follow:

$$\frac{\widehat{s_L^0}}{s_L^0} = \frac{\left(K_r F_r\right)^{1/2} \left(D_{th} F_{th}\right)^{\alpha} \left(D_k F_{sp}\right)^{\beta}}{K_r^{1/2} D_{th}^{\alpha} D_k^{\beta}} = \sqrt{F_r} F_{th}^{\alpha} F_{sp}^{\beta}. \tag{28}$$

The condition $\widehat{s_L^0} = s_L^0$ is fulfilled with the following F_r formulation:

$$F_r = \left[\frac{1}{F_{th}^{\alpha+\beta}} \left(\frac{F_{th}}{F_{sp}} \right)^{\beta} \right]^2 = \frac{1}{F} \left(\frac{F}{F_{sp}} \right)^{2\beta}. \tag{29}$$

In a multi-step reactions chemistry, F_r is applied to all pre-exponential constants. In the classical TF model F_r is equal to $1/F$.

Note that the expressions for F_{th} and F_r (Eqs. (26) and (29)) allow to impose the unstretched flame properties ($k = 0$) for any value of F_{sp}, therefore,

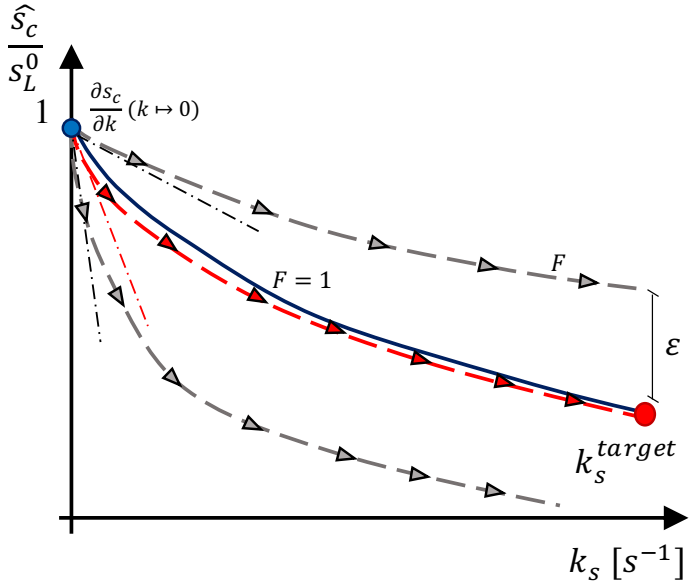

Figure 6: Shooting method applied, by changing the parameter X_0, to retrieve the slope $\frac{\partial s_c}{\partial k}$ for $k \mapsto 0$ such that the constraint in Eq. 30 is accomplished.

the last degree on freedom will be used to identify it. This is accomplished by imposing, as third constraint, that the thickened flame consumption speed at a certain target strain value, k_s^{target}, must match the one obtained from the reference solution at $F = 1$:

$$\widehat{s_c}\left(F > 1, k_s^{target}\right) = s_c\left(F = 1, k_s^{target}\right) \tag{30}$$

In practice, to find the value of F_{sp} that satisfies Eq. (30), we use an optimization procedure based on the following objective function ε:

$$\min_{\frac{\partial s_c}{\partial k}(k_s \mapsto 0)} (\varepsilon) = \min_{\frac{\partial s_c}{\partial k}(k_s \mapsto 0)} \left(\frac{s_c(F=1) - \widehat{s_c}(F)}{s_c(F=1)}\bigg|_{k_s^{target}} \right), \tag{31}$$

where ε measures the difference between the consumption speeds of the flame at $F = 1$ ($s_c(F = 1)$) and at $F > 1$ ($\widehat{s_c}(F)$), evaluated at the target strain

k_s^{target}. An efficient method to minimize ε is to use the slope at $k_s \mapsto 0$ as a shooting parameter to reach $s_c\left(F=1, k_s^{target}\right)$ as shown in Fig. 6. Formally, this slope is influenced by the mixture Lewis number:

$$\frac{\partial s_c}{\partial k} \propto \delta_L^0 \left(Le^0 - 1\right), k_s \mapsto 0 \tag{32}$$

that can be adjusted to match the constraint Eq. (30). Hence, inside the optimization loop, the initial slope $\frac{\partial s_c}{\partial k}$ is changed by modifying the Lewis number $\widehat{Le}$ according to:

$$\left(\widehat{Le} - 1\right) \widehat{\delta_L^0} = \left(Le^0 - 1\right) \delta_L^0 X_0, \tag{33}$$

where X_0 is an optimization function depending on F while the two terms $\left(Le^0 - 1\right) \delta_L^0$ and $\left(\widehat{Le} - 1\right) \widehat{\delta_L^0}$ directly influence the response for $k \mapsto 0$ of the reference solution at $F = 1$ and of the flame transformed by Eq. (23).

Finally, combining Eq. (33) with Eq. (25) gives an expression for the species mass diffusion term F_{sp}:

$$\begin{aligned} F\left(\frac{F_{th} D_{th}}{F_{sp} D_k} - 1\right) &= \left(Le^0 - 1\right) X_0, \\ F_{sp} &= \frac{F_{th} F Le^0}{F + \left(Le^0 - 1\right) X_0}. \end{aligned} \tag{34}$$

Note that F_{sp} depends on F, the mixture Lewis number Le^0 and it is the same for all species.

Eventually, the generalized diffusion-reaction transformation factors are obtained:

$$\begin{cases} F_{th} = F \\ F_{sp} = \frac{F^2 Le^0}{F + (Le^0 - 1) X_0} \\ F_r = \left[\frac{1}{F_{th}^{1/2}} \left(\frac{F_{th}}{F_{sp}}\right)^{\beta}\right]^2 \end{cases} \tag{35}$$

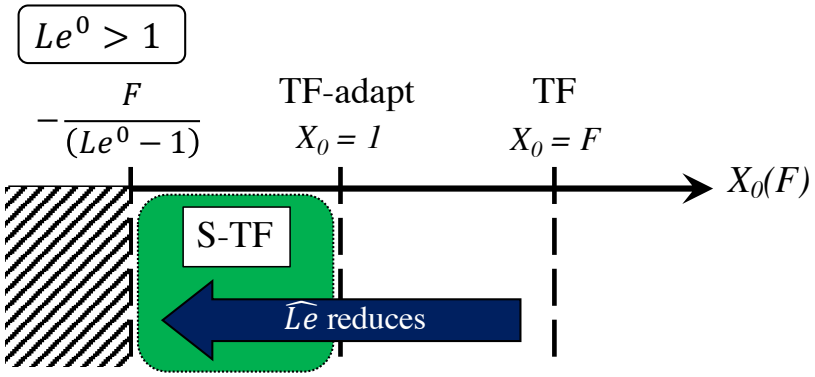

Figure 7: Schematic overview of the three different approaches for $Le^0 - 1 > 0$.

which, after mapping, leads to the Lewis number $\widehat{Le}$:

$$\widehat{Le} = \frac{\widehat{D_{th}}}{\widehat{D_k}} = 1 + \frac{(Le^0 - 1)\, X_0}{F}. \tag{36}$$

Since a positive Lewis number must be ensured, X_0 is limited to:

- If $Le^0 > 1 \longrightarrow X_0 > -\frac{F}{Le^0-1}$
- If $1 > Le^0 > 0 \longrightarrow X_0 < -\frac{F}{Le^0-1}$

Thus, according to the original Lewis number, Le^0, there is one value of X_0, here defined as $\widetilde{X_0}$, that satisfies Eq. (30) for a given value of F, able to correct the stretch response of thickened flames.

Note that Eq. (35) yields a generalized mapping for all thickened flame models, covering different approaches depending on the value assumed by the function X_0 (Fig. 7 for $Le^0 > 1$):

1. $X_0 = F$ yields the Thickened Flame model factors:

$$\begin{cases} F_{th} = F \\ F_{sp} = F \\ F_r = 1/F \end{cases} \tag{37}$$

with $\widehat{Le} = Le^0$.

2. $X_0 = 1$ corresponds to the TF-adapt model:

$$\begin{cases} F_{th} = F \\ F_{sp} = \frac{F^2 Le^0}{F+(Le^0-1)} \\ F_r = \left[\frac{1}{F_{th}^{1/2}}\left(\frac{F_{th}}{F_{sp}}\right)^{\beta}\right]^2 \end{cases} \tag{38}$$

with $\widehat{Le} = 1 + \frac{\left(Le^0-1\right)}{F}$ as expected from TF-adapt theory.

3. $X_0 = \widetilde{X_0}(F)$, with $\widetilde{X_0}(F) \neq 1$ and $\widetilde{X_0}(F) \neq F$, leads to the Stretched-Thickened Flame model, where the $\widetilde{X_0}$ function matches the correct strained flame speed at k_s^{target}, leading to the following mapping factors:

$$\begin{cases} F_{th} = F \\ F_{sp} = \frac{F^2 Le^0}{F+(Le^0-1)\widetilde{X_0}} \\ F_r = \left[\frac{1}{F_{th}^{1/2}}\left(\frac{F_{th}}{F_{sp}}\right)^{\beta}\right]^2 \end{cases} \tag{39}$$

In this case, the Lewis number corresponds to:

$$\widehat{Le} = 1 + \frac{\left(Le^0 - 1\right)\widetilde{X_0}}{F} \tag{40}$$

Note that formally the S-TF model does not guarantee the right slope for $k_s \mapsto 0$ (Markstein number) trying, instead, to match the thickened

flame consumption speed at k_s^{target}. However, once the optimization problem is solved and thickened flame consumption speed matches the one of the reference flame ($F = 1$) at the target stretch value k_s^{target}, $\widehat{s_c}$ will be reasonably predicted also for all strain values below k_s^{target}, since the unstrained solution is recovered by construction and the flame speed response to stretch is usually monotonic between $k_s = 0$ and k_s^{target} (Fig. 6).

It is convenient to choose the target value k_s^{target} in the high strain region to ensure precision over a large range of strain. Note that the definition of k_s^{target} depends on the configuration, even though its exact value is not crucial: it is just used to match the correct thickened flame behavior on an extended set of strain values. In most cases, k_s^{target} can be set to s_L^0/δ_L^0. A more precise approach, followed in this work, is to identify the high strain zone, where the laminar flame response is expected to be non-linear, by using a simple flame case, prone to the extinction strain rate prediction, such as the reactants-to-reactants configuration. In this way, the extinction strain rate, computed for the reference flame at $F = 1$, is able to provide a reasonable region where k_s^{target} can be selected, providing the only input required by the optimization procedure. However, other and more case-dependent solutions can be used. For instance, in explosions [4] the region of interest is limited by the kernel size used to initialize the CFD computation and k_s^{target} may be set to its corresponding stretch value. For the flame in Fig. 5, characterized by a fresh mixture at 1 bar, 300 K and equivalence ratio $\phi = 0.9$, k_s^{target} is fixed to 1450 s^{-1} close to the flame extinction

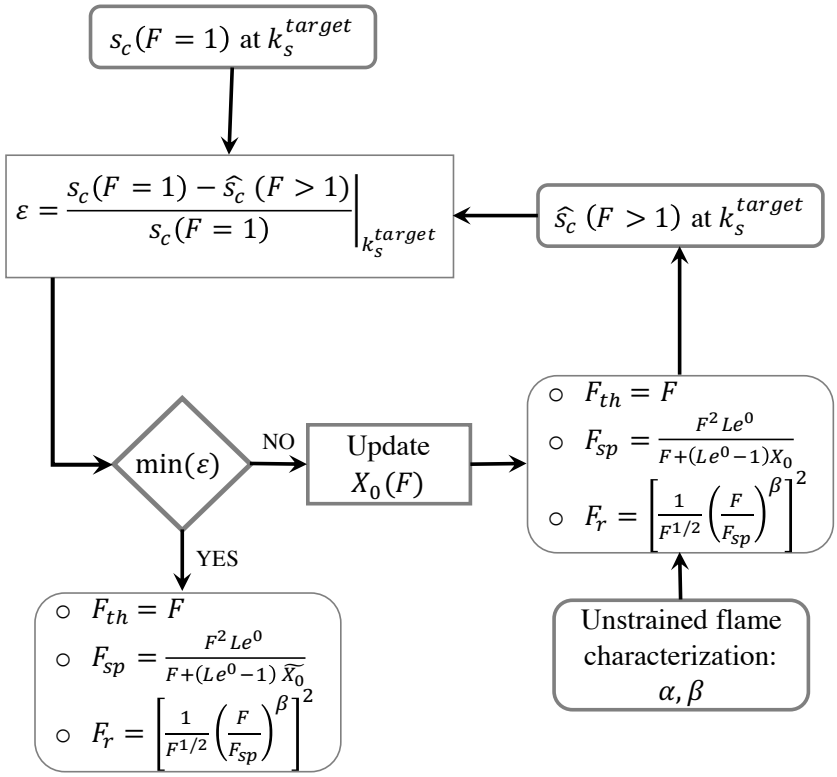

Figure 8: Optimization loop used to obtain S-TF model key parameters F_{th}, F_{sp}, F_r. Consumption speeds of strained flames are computed using the CounterFlow Premixed Flame configuration in CANTERA.

strain rate and order of magnitude of the inverse of the unstretched flame time $s_L^0/\delta_L^0 = 1000\ s^{-1}$.

The procedure to compute $\widetilde{X_0}$ in the Stretched-Thickened Flame model framework is detailed in the next section.

3.2. Optimization procedure

Figure 8 describes the S-TF model optimization loop followed to compute the function $\widetilde{X_0}$ for a certain thickening factor F. Once the fresh gas

conditions have been defined, the code CANTERA[3] is used to simulate both unstrained and strained flames. At first, the 1D unstrained flame behavior is characterized by measuring the parameters α and β of the chemical scheme (see Appendix A). After that, strained flames are computed using the CFPF configuration: the consumption speed of the reference strained flame at $F = 1$ is computed for the chosen k_s^{target} and compared to the value of $\widehat{s_c}(F > 1)$ of the thickened flame for the same strain value. Then the objective function (Eq. (30)) is minimized. It can be done by using different optimization algorithms such as Newton-Raphson, Broyden's or the Differential Evolution (DE) method [44]. Here the DE approach was used since it proved to be the fastest and most effective in converging on a solution, following a stochastic approach in the research of the best candidate, without relying on gradient methods. During this process, X_0 is updated and the curve slope ($\partial s_c/\partial k_s|_{k_s \mapsto 0}$) is modified until the constraint on the burning velocity, $\widehat{s_c}\,(F > 1, k_s^{target}) = s_c\,(F = 1, k_s^{target})$, is satisfied for $X_0 = \widetilde{X_0}$. This process is repeated for different thickening factors, building a $\widetilde{X_0}$ dependency in F as shown in Sect. 4.

In the next section, the results of the optimization procedure are validated for a stagnation point flame and applied to a cylindrical flame configuration.

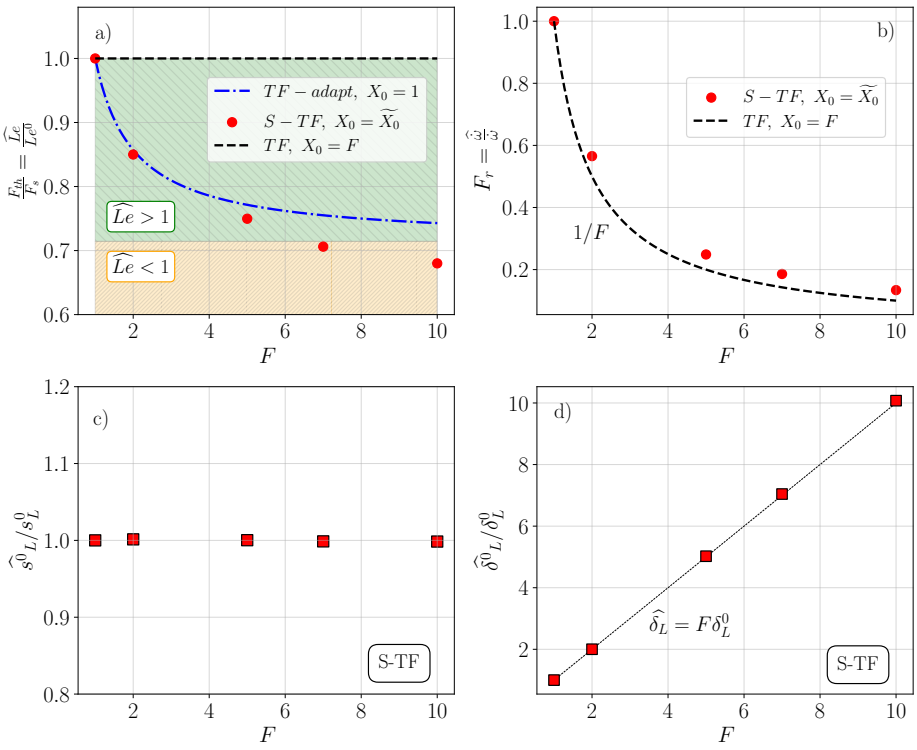

Figure 9: a) Lewis number evolution with the thickening factor for $X_0 = F$ (TF approach), $X_0 = 1$ (TF-adapt approach) and $X_0 = \widetilde{X_0}$ (S-TF approach). b) Pre-exponential correction factor for $X_0 = F$ (TF approach) and $X_0 = \widetilde{X_0}$ (S-TF approach). c) Unstrained laminar flame $\widehat{s_L^0}$ and d) laminar thickness $\widehat{\delta_L^0}$ with S-TF.

4. Stretch-TF model validation and application

4.1. Validation: Stagnation plane flame

Table 4 summarizes the results of the optimization procedure detailed in section 3.2 for a C_3H_8/Air premixed flame obtained with a fresh mixture at $\phi = 0.9$, $P = 1\ bar$ and $T = 300\ K$, using the 2-step chemistry described

[3]The factors F_{th}, F_{sp} and F_r have been implemented in the code CANTERA.

TF model					
F	F_{th}	F_{sp}	F_r	X_0	$\widehat{Le}$
1	1	1	1	1	1.4
2	2	2	0.5	2	1.4
5	5	5	0.2	5	1.4
7	7	7	0.143	7	1.4
10	10	10	0.1	10	1.4

TF-adapt model[4]					
F	F_{th}	F_{sp}	F_r	X_0	$\widehat{Le}$
1	1	1	1	1	1.4
2	2	2.33	0.562	1	1.2
5	5	6.48	0.243	1	1.08
7	7	9.27	0.177	1	1.057
10	10	13.46	0.125	1	1.04

S-TF model					
F	F_{th}	F_{sp}	F_r	X_0	$\widehat{Le}$
1	1	1	1	1	1.4
2	2	2.353	0.565	0.95	1.19
5	5	6.669	0.249	0.62	1.05
7	7	9.913	0.186	-0.2	0.989
10	10	14.706	0.134	-1.2	0.952

Table 4: Thickening scaling factors F, F_{th}, F_{sp}, F_r and the corresponding Lewis number along with the relative X_0 function for the three approaches, TF, TF-adapt, S-TF. Operative conditions: C_3H_8/Air at 300 K, 1 bar and $\phi = 0.9$.

in Sect. 2.2. The thickening factors (F_{th}, F_{sp}, F_r), the X_0 function and the modified Lewis numbers obtained with the TF, TF-adapt and S-TF models are compared. The S-TF approach reduces the Lewis number when the thickening factor increases and diverges from the TF-adapt when the actual strain Fk_s that the flame experiences is higher, as reported in Fig. 9a. Figure 9b shows that while the Lewis number is decreasing, the pre-exponential factor is modified. Although F_r differs from the simple $1/F$ function of the Thick-

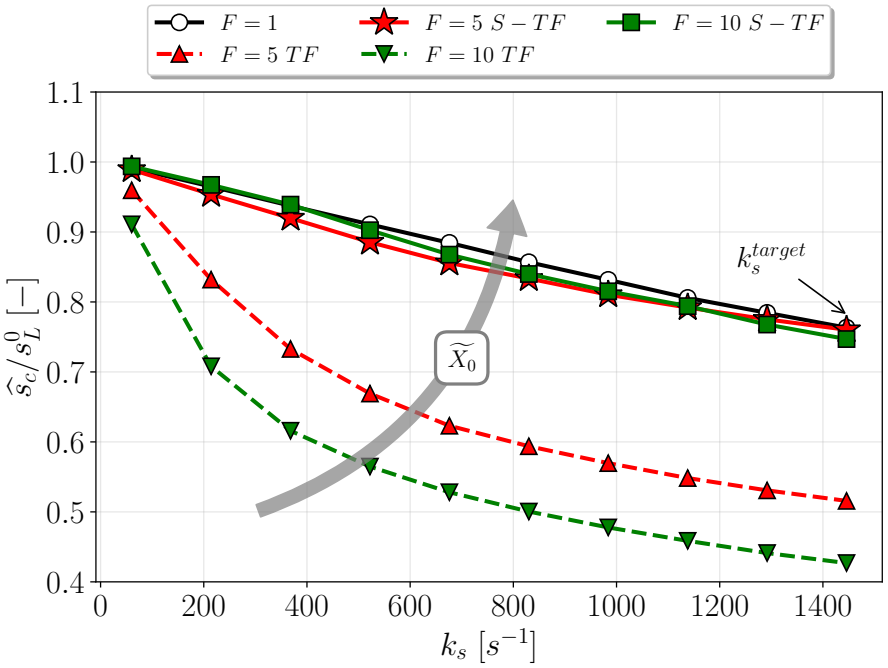

Figure 10: Consumption speed of C_3H_8/Air flame computed with S-TF and TF approaches. Operative conditions: $P = 1\ bar$, $T = 300\ K$ and $\phi = 0.9$.

ened Flame model, S-TF provides the same results in terms of unstretched laminar flame parameters: $\widehat{s_L^0}$ is conserved and $\widehat{\delta_L^0}$ is scaled by a factor F (Fig. 9c and Fig. 9d).

Figure 10 shows the consumption speed variation of 1D strained flames when thickened using the S-TF models with $F = 5$ and $F = 10$, compared with the $F = 1$ flame. For each flame, the optimization strategy of 3.2 is used to define $\widetilde{X_0}$. Figure 10 also reports the prediction of the TF model (dashed lines) to highlight the S-TF model impact. As expected, at the optimization point ($k_s = k_s^{target}$), the 50% error obtained with the classical TF model is fully corrected by the S-TF model. A good match on s_c is also achieved

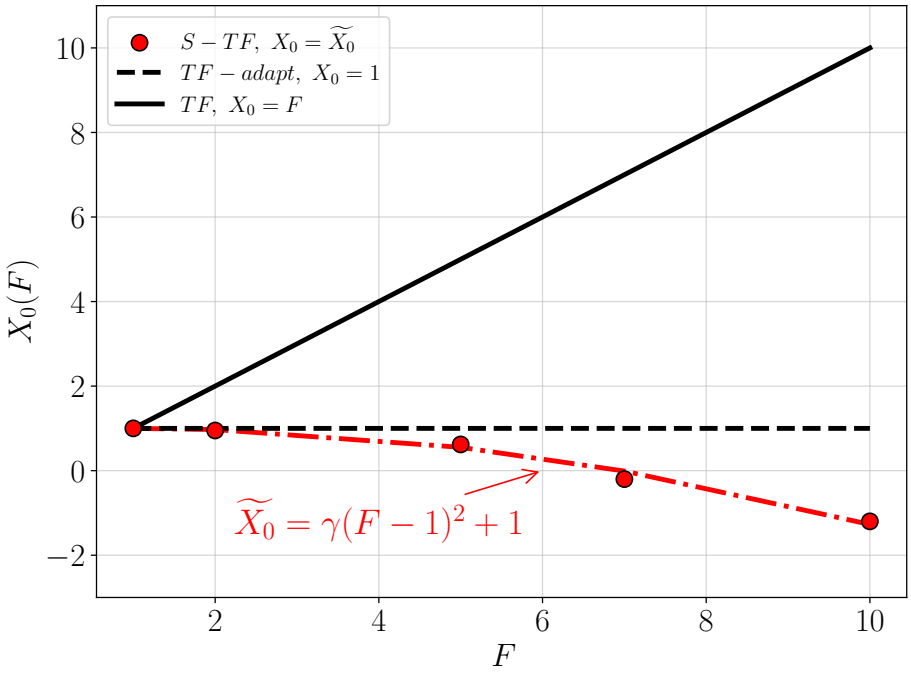

Figure 11: X_0 function behavior with the thickening factor F for TF model ($X_0 = F$), TF-adapt ($X_0 = 1$) and S-TF ($X_0 = \widetilde{X_0}$). $\widetilde{X_0}$ obtained for C_3H_8/Air flame at $P = 1$ *bar*, $T = 300$ *K* and $\phi = 0.9$.

at other k_s values, without the need to repeat the optimization process at different k_s^{target}.

In addition, for all F values, at weakly strained regime, the consumption speed, $\widehat{s_c}$, tends towards the laminar flame speed s_L^0, proving that the constraint of Eq. (24) is also well verified by construction of the model (Eq. (24) and (25)).

The evolution of $\widetilde{X_0}$ derived by the optimization process at different thickening factors F is shown in Fig. 11 for the C_3H_8/Air flame at $P = 1$ *bar*, $T = 300$ *K* and $\phi = 0.9$. The values obtained lie around a parabolic trend

with amplitude $\gamma = -0.03$. $\widetilde{X_0}$ becomes also negative and the chemistry Lewis number is pushed towards values lower than one. The γ parameter depends only on the mixture conditions (P, T, ϕ) and allows to represent the F-dependent correction with a simple analytical function $\widetilde{X_0}$ that can be easily implemented in a CFD code. As an example, Appendix C provides a list of γ values for the C_3H_8/Air flame obtained for $P = 1\ bar$, $T = 300\ K$ and different values of ϕ. The procedure to obtain γ for other conditions is also described. In particular, once the function $\widetilde{X_0}$ is known for given mixture conditions, it can be applied without requiring any information about the strain rate (or the range of strain rates) acting on the flame. This is not a minor aspect because during a complex CFD simulation, if the S-TF model is applied, the flame elements, when thickened, will react correctly whether they are strained or not, without any evaluation of the local strain acting on the reaction front.

Figure 12 displays normalized temperature θ (Eq. (5)) versus normalized fuel mass fraction:

$$\Psi = \frac{Y_F - Y_F^b}{Y_F^u - Y_F^b} \tag{41}$$

at $k_s = 1450\ s^{-1}$ for $F = 1$, $F = 5$ and $F = 10$. When the Thickened Flame model is applied, species and thermal diffusion are scaled by the same parameter F, thus, the relative diffusion of species and heat is kept constant with the thickening factor. As a consequence, the profiles of $\widehat{\Psi}$ are superimposed if evaluated in the temperature domain (Fig. 12b). Conversely, with the S-TF approach (Fig. 12a), species diffusion is amplified more than temperature diffusion since the generalization of the diffusion-reaction transformation yields $F_{sp} > F_{th}$ when $Le^0 > 1$. For this reason, using the S-TF model, $\widehat{\Psi}$ reduces

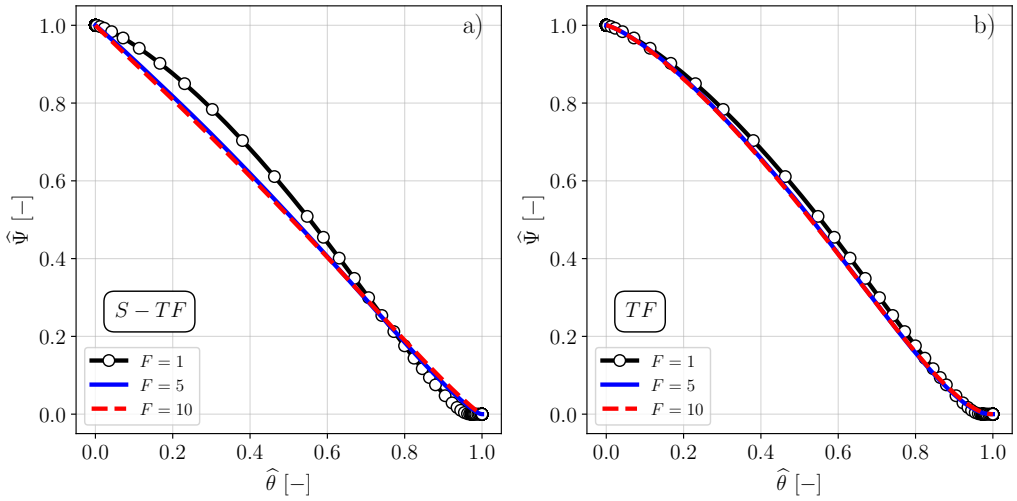

Figure 12: Normalized fuel mass fraction $\widehat{\Psi}$ plotted against the normalized temperature $\widehat{\theta}$ with the S-TF approach for $k_s = 1450\ s^{-1}$ a) and with the TF approach b).

with the thickening factor for each value of $\widehat{\theta}$ and tends to $\widehat{\Psi} + \widehat{\theta} = 1$ profiles, in accordance with the optimized Lewis number $\widehat{Le}$ close to unity. The improvement in thickened flame response is further confirmed in Fig. 13 where the profiles of $\widehat{\dot{\omega}} F_r / \left(\widehat{\nabla\theta}\right)$ and $\widehat{\dot{\omega}} / \left(\widehat{F\nabla\theta}\right)$ are evaluated in temperature space. The integral of these functions determines the consumption speed (Eq. (8)) and proves that the TF approach underestimates it (Fig. 13b) while the S-TF model approaches the reference solution (Fig. 13a).

4.2. Application: Cylindrical expanding flame

In this section, the S-TF model is applied to a 2D cylindrical expanding flame (Fig. 14a). Here, the laminar flame is subjected to pure curvature, namely $k_c = \frac{1}{r_b}\frac{dr_b}{dt}$, where r_b is the radius of the burnt products region. Although this flame is only curved, the S-TF model is used without any modification to show that, even though it uses a 1D strained flame as a

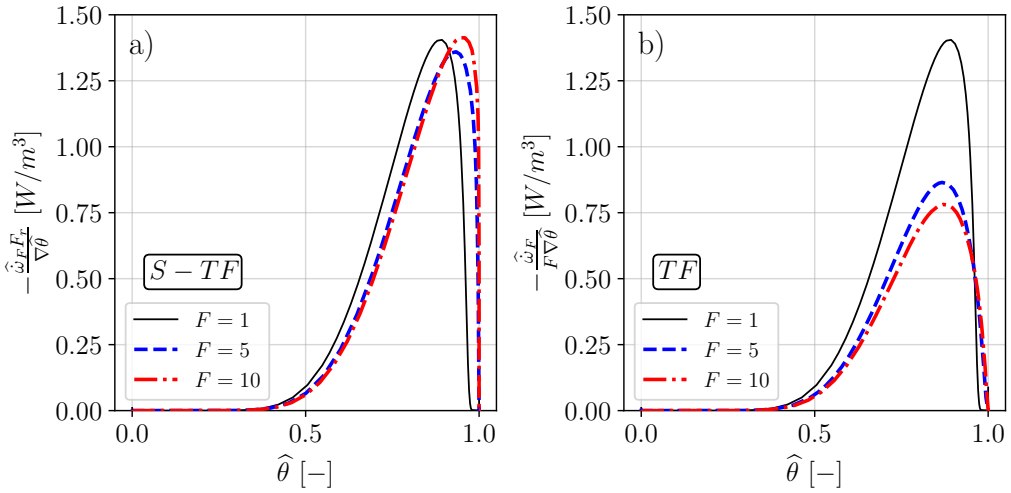

Figure 13: a) Flame structure with S-TF model. b) Flame structure with TF model. $k_s = 1450\ s^{-1}$.

reference configuration for the optimization procedure, it propagates all flame elements (strained or curved), potentially present in a turbulent flame brush, at the right speed. In addition, while the flame expands in time, its curvature changes according to r_b and the S-TF model can be tested over a wide range of k_c.

Simulations are carried out using the high-fidelity compressible LES solver *AVBP* (http://www.cerfacs.fr/avbp7x/). The fresh mixture conditions are the same used for the CounterFlow Premixed Flame (C_3H_8/Air mixture at $P = 1\ bar, T = 300\ K, \phi = 0.9$) and ignited using the Energy Deposition model (ED model) [7]. Two different grids are used to target $F = 1$ and $F = 10$ (Fig. 14c). As shown in Fig. 14(b-c), the flames are initialized at the origin of the domain (Fig. 14a) in a refined region with $\Delta x = 60\mu m$, corresponding to unity thickening factor ($F = 1$), such that all flames are

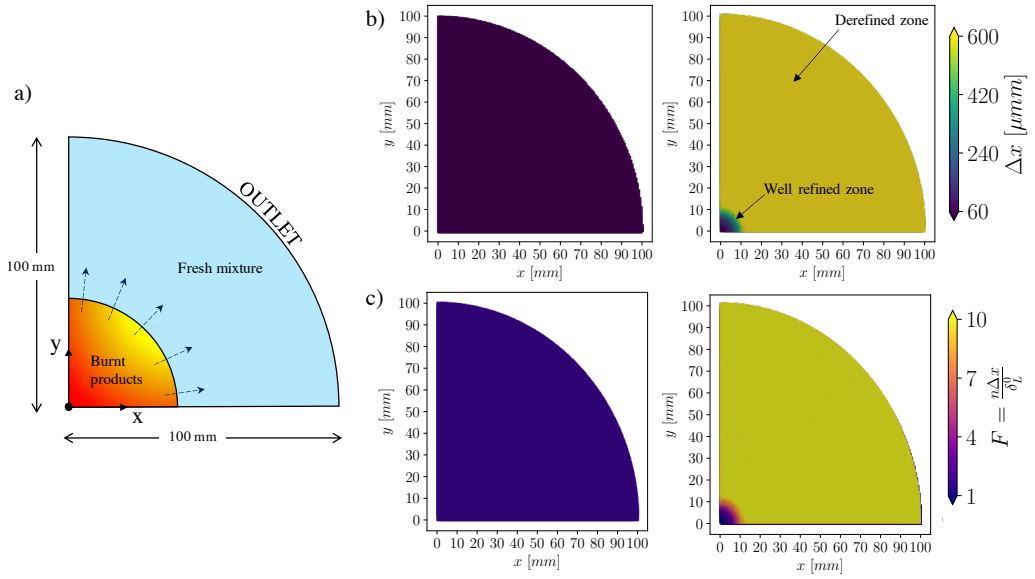

Figure 14: a) 2D cylindrical expanding flame. It is initialized in $x = 0$, $y = 0$ and it propagates in a quarter-circle shaped domain. b) Mesh size for the two cases: $F = 1$ and $F = 10$ c) A priori thickening factor field accounting seven points in the flame front. The laminar flame thickness is equal to 0.42 mm for a fresh mixture at 1 bar, 300 K, $\phi = 0.9$.

ignited in the same well resolved zone and later enter a coarser grid region where thickening is applied depending to the grid size (Fig. 14c). Thus, the chosen configuration is as close as possible to most LES simulation where thickening is controlled by the local cells dimension. The thickening factor is computed relying on the dynamic version of the TF model (DTFLES [45]):

$$F = \frac{n\Delta x}{\delta_L^0}, \tag{42}$$

where $n = 7$ is the number of points used to resolve the flame structure [46] and Δx is the mesh size.

The parabolic function shown in Fig. 11 is implemented in the code to take the thickening variations into account and correct the Lewis number

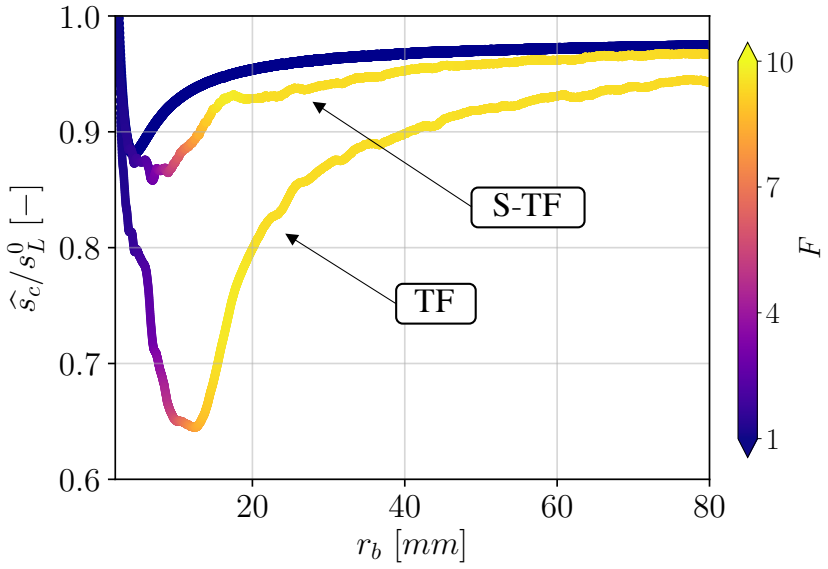

Figure 15: Cylindrical flame consumption speed colored with the thickening factor. Comparison between cases at $F = 1$ and $F = 10$. C_3H_8/Air flame at $P = 1$ bar, $T = 300$ K and $\phi = 0.9$.

consequently. The code computes the local thickening value as in the classical Thickened Flame model and attributes a value to the pre-computed F-function $\widetilde{X_0}(F)$. In this way, F_{th}, F_{sp} and F_r are evaluated and applied to the diffusion coefficients and the source terms. This process is detailed in Appendix B.

The consumption speed is computed by measuring the flame surface A_f and integrating the rate of the reactant consumption through the entire surface $\int_\Sigma \dot{\omega}_F d\Sigma$ [37]:

$$s_c = -\frac{1}{A_f \left(Y_F^u - Y_F^b\right) \rho^u} \int_\Sigma \dot{\omega}_F d\Sigma. \tag{43}$$

The flame surface A_f is evaluated using the area covered by the burnt

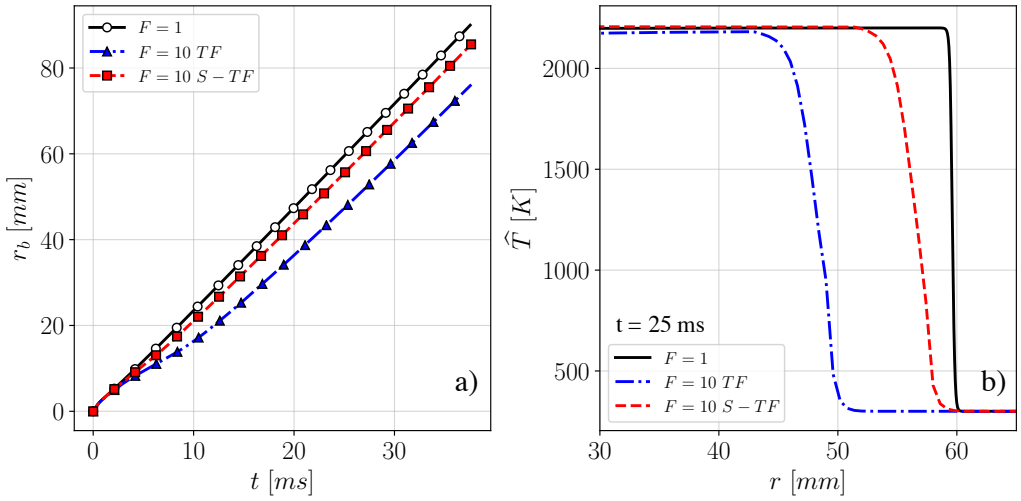

Figure 16: a) Radius of the kernels burnt products evolution in time by using the TF model and the S-TF model. Comparison with $F = 1$ flame. b) Flame structure at $t = 25\ ms$: temperature profile $\widehat{T}$ over the flame radius computed with the TF and the S-TF model. Comparison with the $F = 1$ flame.

products, estimated as the integral of the progress variable θ on the computational domain:

$$Q_b = \int_\Sigma \theta d\Sigma. \tag{44}$$

The radius r_b is deduced from the surface of burnt gases Q_b using $Q_b = \pi r_b^2$ in this 2D configuration.

Figure 15 displays the flame consumption speed as a function of the radius r_b. The fully resolved flame ($F = 1$) is useful to understand the flame dynamics: during the early instants after ignition, the consumption rate increases quickly and fresh gases are burnt faster then the laminar speed s_L^0. This is due to the spark energy that influences the flame dynamics in the first moment of ignition [47], until a small kernel of burnt products is generated

and starts growing. Since the flame is highly stretched, the consumption speed decreases to $s_c \approx 88\% s_L^0$ when $r_b \approx 4\ mm$. Then, k_c reduces in time and the flame burning velocity tends to the laminar flame speed at high r_b [47]. When the flame moves on a coarser grid, it is thickened and starts experiencing F times the actual stretch acting on $F = 1$ flame. For this reason, as soon as the TF model mapping (Eq. (7)) is applied, at small radius (high curvature) the stretch effect is amplified and the consumption speed is drastically reduced. In this case the error on the predicted $\widehat{s_c}$ relative to the reference consumption speed is higher than 30% (Fig. 15) and the $s_c(F = 1)$ is reached at $r_b = 70\ mm$.

The S-TF model compensates for this, leading to a flame which propagates almost like the flame at $F = 1$. When the S-TF model is applied, the consumption speed reaches the target value at $r_b < 20\ mm$ and the exact flame behavior is quickly recovered. As a consequence, the flame position over time is better predicted compared to the classical Thickened Flame model as shown in Fig. 16a where the flame radius is monitored in time. As long as the flame front propagates on the coarser mesh, flame resolved by the TF model is slowed down by curvature, while the S-TF approach keeps it close to the reference case ($F = 1$). Then, when the k_c effects become negligible, all flame fronts move at the same absolute speed $r_b^{'} \approx \rho^u/\rho^b s_L^0$. Even if the stretch changes in time, the S-TF model is able to reproduce the correct evolution of the flame burning velocity since the model parameters, found in the strained flame configuration, provide the s_c correction over a wide range of k_s.

Figure 16b illustrates the temperature profiles traced at $t = 25\ ms$ along

the flame radius. The thermal thickness of the flame resolved with the TF and the S-TF model is increased by the same quantity since $F_{th} = F$, ensuring the same resolution. However the S-TF model increases the mass diffusion thickness such that, with a $\widehat{Le} = 0.95$ (Table 4), the corresponding flame moves closer to the flame at $F = 1$, describing its evolution more accurately. The Stretched-Thickened flame model provides also a better prediction of the flame temperature. The asymptotic theory [28, 29] reveals that also the temperature reached in the reaction zone depends on the factor $(Le^0 - 1)$ [37], as obtained for the consumption speed s_c (Eq. 21). As a consequence, the proposed Lewis number modification allows to preserve at the same time not only the burning velocity but also the flame temperature of a stretched thickened flame, without any additional constraint.

5. Conclusions

In this work a strategy to capture the stretch response of flames, thickened using the Thickened Flame model is proposed. As shown in previous works [19], the mathematical analysis of a planar flame in a stagnation point flow highlights the need to revise the diffusion-reaction transformation which the Thickened Flame model is based on. This is achieved by modifying the thermal and species diffusivity with different factors as well as adjusting the pre-exponential constants to match specific flame properties.

At first, the diffusion-reaction transformation is generalized and the scaling factor applied on the thermal and species mass diffusion as well as on the reaction terms are computed to ensure the laminar flame speed conservation, the thermal thickness resolution and the same stretch response between

thickened and non thickened flame. In the last constraint, an optimization function is included to match the stretched flame speed at one large stretch value k_s of the order of s_L^0/δ_L^0.

The 1D flame, strained in a stagnation point flow, is used as reference case to validate the optimization procedure, ensuring a correct flame response in a large range of strain, from weak to high values. Then the optimized diffusion-reaction transformation developed for strained flames is used for the cylindrical flame configuration where only curvature acts. At small kernel radii the flame consumption speed is enhanced and the flame dynamics in time is much better with the S-TF approach.

The described model suggests a practical solution to overcome TF model limits for stretched flames, without requiring local stretch computation or discrimination between strained, curved or unstretched flame during the simulation. From an implementation point of view, the S-TF model preserves the simplicity of the TF approach and offers a viable solution for complex CFD codes.

Concerning stretched turbulent flames, the prediction of the turbulent speed $s_T = Es_c$ can benefit from the S-TF model, which would guarantee the correct burning velocity s_c of all stretched segments composing the flame front. Added up to the subgrid turbulence model E [1, 22, 23], the Stretched-Thickened Flame model represents a further step towards increasingly reliable turbulent combustion models.

Acknowledgements and Fundings

This project has received funding from the European Union's Horizon 2020 research and innovation program under Grant Agreement No 956803 (INSPIRE - INSpiring Pressure gain combustion Integration, Research, and Education). This work was performed using HPC resources from GENCI-TGCC (Grant 2023 - A0132B10157)

References

[1] O. Colin, F. Ducros, D. Veynante, T. Poinsot, A thickened flame model for large eddy simulations of turbulent premixed combustion, Phys. Fluids 12 (2000) 1843–1863.

[2] P. J. O'Rourke, F. V. Bracco, Two scaling transformations for the numerical computation of multidimensional unsteady laminar flames, J. Comput. Phys. 33 (1979) 185–203.

[3] P. S. Volpiani, T. Schmitt, D. Veynante, Large Eddy Simulation of a turbulent swirling premixed flame coupling the TFLES model with a dynamic wrinkling formulation, Combust. Flame 180 (2017) 124–135.

[4] P. S. Volpiani, T. Schmitt, O. Vermorel, P. Quillatre, D. Veynante, Large Eddy Simulation of explosion deflagrating flames using a dynamic wrinkling formulation, Combust. Flame 186 (2017) 17–31.

[5] G. Wang, M. Boileau, D. Veynante, Implementation of a dynamic thickened flame model for Large Eddy Simulations of turbulent premixed combustion, Combust. Flame 158 (2011) 2199–2213.

[6] O. Vermorel, P. Quillatre, T. Poinsot, LES of explosions in venting chamber: A test case for premixed turbulent combustion models, Combust. Flame 183 (2017) 207–223.

[7] G. Lacaze, E. Richardson, T. Poinsot, Large Eddy Simulation of spark ignition in a turbulent methane jet, Combust. Flame 156 (2009) 1993–2009.

[8] E. Sandoval Garzon, C. Mehl, O. Colin, Modeling of spark ignition in gaseous mixtures using adaptive mesh refinement coupled to the thickened flame model, Combust. Flame 248 (2023) 112507.

[9] P. Agostinelli, D. Laera, I. Chterev, I. Boxx, L. Gicquel, T. Poinsot, Large eddy simulation of mean pressure and $H2$ addition effects on the stabilization and dynamics of a partially-premixed swirled-stabilized methane flame, Combust. Flame 249 (2023) 112592.

[10] D. Laera, P. W. Agostinelli, L. Selle, Q. Cazères, G. Oztarlik, T. Schuller, L. Gicquel, T. Poinsot, Stabilization mechanisms of CH4 premixed swirled flame enriched with a non-premixed hydrogen injection, Proc. Combust. Inst. 38 (2021) 6355–6363.

[11] W. Han, H. Wang, G. Kuenne, E. R. Hawkes, J. H. Chen, J. Janicka, C. Hasse, Large Eddy Simulation of dynamic thickened flame modeling of a high Karlovitz number turbulent premixed jet flame 37 (2019) 2555–2563.

[12] G. Kuenne, A. Ketelheun, J. Janicka, LES modeling of premixed com-

bustion using a thickened flame approach coupled with FGM tabulated chemistry, Combust. Flame 158 (2011) 1750–1767.

[13] V. Granet, O. Vermorel, C. Lacour, B. Enaux, V. Dugué, T. Poinsot, Large Eddy Simulation and experimental study of cycle-to-cycle variations of stable and unstable operating points in a spark ignition engine, Combust. Flame 159 (2012) 1562–1575.

[14] S. J. Kazmouz, D. C. Haworth, P. Lillo, V. Sick, Extension of a thickened flame model to highly stratified combustion—Application to a spark-ignition engine, Combust. Flame 236 (2022) 111798.

[15] A. Misdariis, O. Vermorel, T. Poinsot, LES of knocking in engines using dual heat transfer and two-step reduced schemes, Combust. Flame 162 (2015) 4304–4312.

[16] H. Terashima, Y. Hanada, S. Kawai, A localized thickened flame model for simulations of flame propagation and autoignition under elevated pressure conditions, Proc. Combust. Inst. 000 (2020) 1–8.

[17] M. Boileau, G. Staffelbach, B. Cuenot, T. Poinsot, C. Bérat, LES of an ignition sequence in a gas turbine engine, Combust. Flame 154 (2008) 2–22.

[18] D. Veynante, T. Poinsot, Large Eddy Simulation of combustion instabilities in turbulent premixed burners, Proc. Summer Program, Cent. Turbul. Res. (1997) 253–275.

[19] S. Popp, G. Kuenne, J. Janicka, C. Hasse, An extended artificial thickening approach for strained premixed flames, Combust. Flame 206 (2019) 252–265.

[20] F. Proch, A. M. Kempf, Modeling heat loss effects in the large eddy simulation of a model gas turbine combustor with premixed flamelet generated manifolds, Proc. Combust. Inst. 35 (2015) 3337–3345.

[21] A. L. Comer, T. P. Gallagher, K. Duraisamy, B. A. Rankin, A modified thickened flame model for simulating extinction, Combust. Theor. Model 26 (2022) 1–31.

[22] F. Charlette, C. Meneveau, D. Veynante, A power-law flame wrinkling model for LES of premixed turbulent combustion Part I: Non-dynamic formulation and initial tests, Combust. Flame 131 (2002) 159–180.

[23] F. Charlette, C. Meneveau, D. Veynante, A power-law flame wrinkling model for LES of premixed turbulent combustion Part II: Dynamic Formulation, Combust. Flame 131 (2002) 181–197.

[24] T. Poinsot, D. Veynante, Theoretical and numerical combustion, Amazon, 2022.

[25] S. Poncet, C. Mehl, K. Truffin, O. Colin, Modified diffusion model adapted to non-unity Lewis number mixtures for low flame stretch using the thickened flame model, 11st European Combustion Meeting (2023), paper 439922.

[26] E. Knudsen, H. Kolla, E. R. Hawkes, H. Pitsch, LES of a premixed jet

flame DNS using a strained flamelet model, Combust. Flame 160 (2013) 2911–2927.

[27] T. D. Butler, P. J. O'Rourke, A numerical method for two dimensional unsteady reacting flows, Symp. (Int.) Combust. 16 (1977) 1503–1515.

[28] W. B. Bush, F. E. Fendell, Asymptotic analysis of laminar flame propagation for general Lewis numbers, Combust. Sci. Technol. 1 (1970) 421–428.

[29] P. Clavin, G. Joulin, Premixed flames in large scale and high intensity turbulent flow, J. Phys. Lett-Paris 44 (1983) 1–12.

[30] G. H. Markstein, Non-steady Flame Propagation Pergamon, Elsevier, 1964.

[31] C. J. Sun, C. J. Sung, L. He, C. K. Law, Dynamics of weakly stretched flames: Quantitative description and extraction of global flame parameters, Combust. Flame 118 (1999) 108–128.

[32] M. Matalon, C. Cui, J. K. Bechtold, Hydrodynamic theory of premixed flames: Effects of stoichiometry, variable transport coefficients and arbitrary reaction orders, J. Fluid Mech. 487 (2003) 179–210.

[33] P. Clavin, P. Garcia, The influence of the temperature dependence of diffusivities on the dynamics of flame fronts, J. Mec. Theor. Appl. 2 (1983) 245–263.

[34] J. K. Bechtold, M. Matalon, Hydrodynamic and diffusion effects on the

stability of spherically expanding flames, Combust. Flame 67 (1987) 77–90.

[35] P. Pelce, P. Clavin, Influence of hydrodynamics and diffusion upon the stability limits of laminar premixed flames, J. Fluid Mech. 124 (1982) 219–237.

[36] J. K. Bechtold, M. Matalon, The dependence of the Markstein length on stoichiometry, Combust. Flame 127 (2001) 1906–1913.

[37] G. K. Giannakopoulos, C. E. Frouzakis, S. Mohan, A. G. Tomboulides, M. Matalon, Consumption and displacement speeds of stretched premixed flames - Theory and simulations, Combust. Flame 208 (2019) 164–181.

[38] E. R. Hawkes, J. H. Chen, Comparison of direct numerical simulation of lean premixed methane-air flames with strained laminar flame calculations, Combust. Flame 144 (2006) 112–125.

[39] N. Detomaso, D. Laera, P. Pouech, F. Duchaine, T. Poinsot, Large Eddy Simulation of a pistonless constant volume combustor: a new concept of pressure gain combustion, J. Eng. Gas Turb. Power 145 (2023) 1–10.

[40] B. Franzelli, E. Riber, M. Sanjosé, T. Poinsot, A two-step chemical scheme for kerosene-air premixed flames, Combust. Flame 157 (2010) 1364–1373.

[41] B. Franzelli, E. Riber, L. Y. Gicquel, T. Poinsot, Large Eddy Simulation of combustion instabilities in a lean partially premixed swirled flame, Combust. Flame 159 (2012) 621–637.

[42] F. Frenklach, H. Wang, C.-L. Yu, M. Goldenberg, C. Bowman, R. Hanson, D. Davidson, E. Chang, G. Smith, D. Golden, W. Gardiner, V. Lissianski, The GRI 3.0 chemical kinetic mechanism (1999).

[43] P. Clavin, G. Searby, Combustion waves and fronts in flows: flames, shocks, detonations, ablation fronts and explosion of stars, Cambridge University Press, 2016.

[44] R. Storn, K. Price, Differential Evolution - A simple and efficient heuristic for global optimization over continuous spaces, J. Global Optim. 11 (1997) 341–359.

[45] J. P. Legier, T. Poinsot, D. Veynante, Dynamically thickened flame LES model for premixed and non-premixed turbulent combustion, Proc. Summer Program, Cent. Turbul. Res. (2000) 157–168.

[46] B. Rochette, F. Collin-Bastiani, L. Gicquel, O. Vermorel, D. Veynante, T. Poinsot, Influence of chemical schemes, numerical method and dynamic turbulent combustion modeling on LES of premixed turbulent flames, Combust. Flame 191 (2018) 417–430.

[47] A. P. Kelley, C. K. Law, Nonlinear effects in the extraction of laminar flame speeds from expanding spherical flames, Combust. Flame 156 (9) (2009) 1844–1851.

[48] K. Kuo Kenneth, Principles of combustion, John Wiley & Sons, 2006.

Supplementary Materials

Appendix A

The premixed flame theory [24, 43, 48] provides the analytical expression of the laminar flame speed for a $n-$order reaction:

$$s_L^0 \propto \sqrt{K_r D_{th} Le^n} = K_r^{1/2} D_{th}^{\frac{n+1}{2}} D_k^{-\frac{n}{2}} \tag{45}$$

where K_r is the reaction pre-exponential factor, D_{th} is the thermal diffusion and D_k is the species mass diffusion. It is effective under strict hypothesis and may not be accurate for more complex chemistries with multiple reactions. A more flexible approach is proposed to obtain the correct laminar flame speed dependency on thermal diffusion and species mass diffusion for the specific chemical mechanism chosen. Eq. (45) is recast as:

$$s_L^0 \propto K_r^{1/2} D_{th}^{\alpha} D_k^{\beta} \tag{46}$$

with α and β, parameters describing the physics of the laminar unstrained flame, generalizing the dependency on D_{th} and D_k. Note that they are linked to each other and Eq. (45) suggests that their sum is equal to 1/2. These two parameters depend on the flame and can be obtained by perturbing the laminar premixed flame with a variation of either D_{th} or D_k. According to Eq. (46), when the thermal diffusion coefficient of the mixture is modified by a factor ϵ_{th}, the laminar flame speed responds as follow:

$$\begin{aligned} \frac{s_L^{'}}{s_L^0} &= \epsilon_{th}^{\alpha} \\ \longrightarrow ln\left(\frac{s_L^{'}}{s_L^0}\right) &= \alpha ln(\epsilon_{th}) \end{aligned} \tag{47}$$

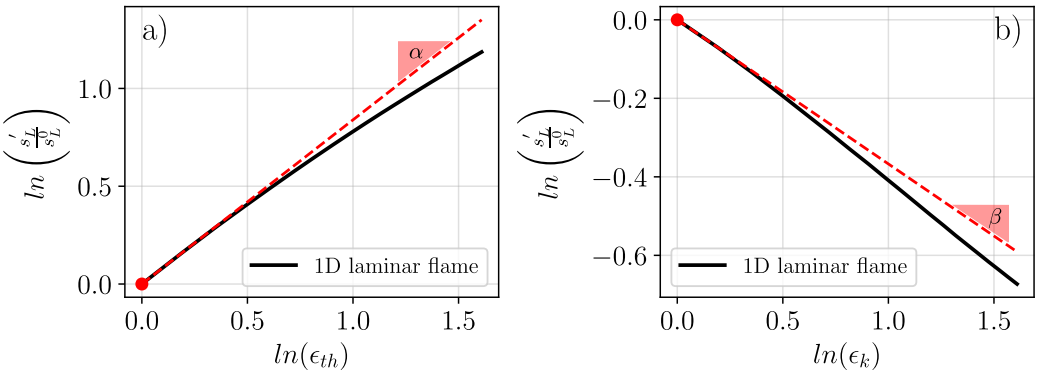

Figure 17: a) Laminar flame speed evolution with thermal diffusion variation (—). b) Laminar flame speed evolution with species mass diffusion variation (—). The tangent lines (- - -) represent the flame behavior for small perturbations.

In a logarithmic domain it corresponds to a linear function with slope α. In the same way, by altering the species mass diffusion D_k with a factor ϵ_k yields:

$$\begin{aligned} \frac{s'_L}{s^0_L} &= \epsilon_k^{\beta} \\ \longrightarrow ln\left(\frac{s'_L}{s^0_L}\right) &= \beta ln(\epsilon_k) \end{aligned} \tag{48}$$

Fig. 17 shows how the laminar flame reacts with changes of thermal diffusion (Fig. 17a) or species mass diffusion (Fig. 17b). In the small perturbations region, the flame reacts following exactly the power law (Eq. (46)) suggested by the premixed flame theory: in logarithmic domain, the response is linear and its slope represents the flame behavior in the parameters D_{th} and D_k.

For the two-step chemistry used in the paper (Sect. 2) and for a fresh mixture at $1bar$, $300K$ at $\phi = 0.9$, $\alpha = 0.879$ and $\beta = -0.378$. α and β describes the flame behavior and depends on the chemical mechanism used. Their sum is equal to 0.5 as expected from premixed flame theory. This

implies that only the computation of one on them is required.

Note that the methodology proposed is independent of the complexity of the chemical mechanism and allows to obtain numerically the mixture global reactivity for certain operative conditions.

Appendix B

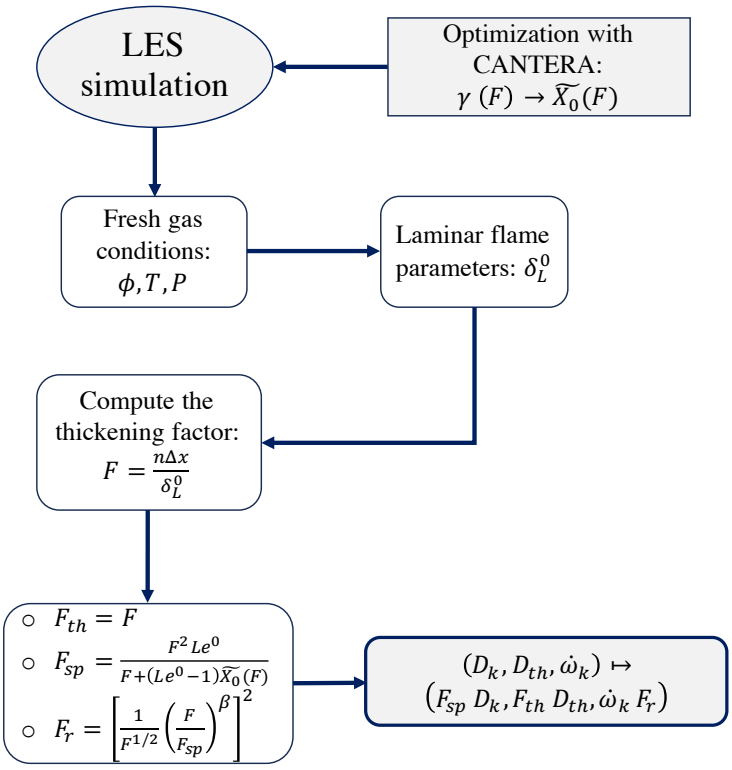

Figure 18: Schematic flow chart describing the actual application of the S-TF model in a CFD code.

Figure 18 illustrates the procedure followed to implement the Stretched-Thickened Flame model in a CFD code.

Once the k_s^{target} is defined (usually $k_s^{target} \approx s_L^0/\delta_L^0$) following the approach proposed in the paper, the CounterFlow Premixed Flame configuration is used to find the function $\widetilde{X_0}$ or the parameter γ describing the F-dependency, (refer to Fig. 11 in the paper) for given operative conditions, able to optimize the chemistry Lewis number and correct the stretched thickened flame behavior. During the simulation runtime, the laminar unstrained flame prop-

erties, e.g., δ_L^0 are used to obtain the thickening factor F, as proposed by the Dynamic Thickened Flame model formulation [45]. At this point, the parameters defined for the generalized diffusion-reaction transformation, F_{th}, F_{sp} and F_r are computed and applied respectively to the thermal diffusion coefficient D_{th}, the species mass diffusion D_k and the species source terms.

Appendix C

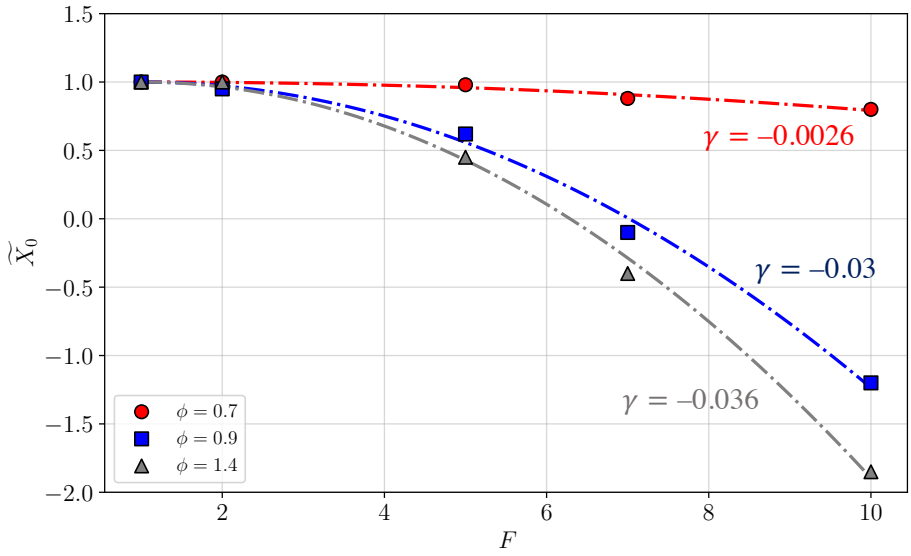

Figure 19: $\widetilde{X_0}$ function behavior with the thickening factor F for Stretch-Thickened Flame model. $\widetilde{X_0}$ obtained for C_3H_8/Air flame at $P = 1\ bar$, $T = 300\ K$ and $\phi = 0.7/0.9/1.4$.

Figure 19 illustrates the $\widetilde{X_0}(F)$ function computed for the C_3H_8/Air mixture at $P = 1\ bar$, $T = 300\ K$ for $\phi = 0.7/0.9/1.4$. As highlighted in the paper, $\widetilde{X_0}(F)$ values, obtained from Eq. (30), lie around the following parabolic fit:

$$\widetilde{X_0} = \gamma\,(F-1)^2 + 1. \tag{49}$$

Equation 49 is such that for $F = 1$, $\widetilde{X_0}(F = 1) = 1$ and the factors of the generalize mapping in Eq. (23) become equal to one:

$$\begin{cases} F_{th} = 1 \\ F_{sp} = 1 \\ F_r = 1 \end{cases} \tag{50}$$

Increasing the values of F, the S-TF function $\widetilde{X_0}$ diverges from the X_0 corresponding to TF-adapt ($X_0 = 1$) since the flame experiences an higher strain Fk_s and TF-adapt hypotheses do not hold anymore.

γ is the curve amplitude that minimizes the distance between all the optimized values $\widetilde{X_0}(F)$. Its definition is convenient when the model is implemented in a CFD code: during an LES simulation, if F changes locally due to, for example, mesh size (see Section 4.2 and Eq. (42)), it is useful to reduce the number of parameters that have to be implemented in the code. The F-function $\widetilde{X_0}$ modelled as in Eq. (49), once defined γ, requires only the thickening factor F to modify the mixture Lewis number accordingly and correct the stretch response of the computed thickened flame.